

A Study on Prenucleation and Heterogeneous Nucleation in Liquid Pb on Solid Al using Molecular Dynamics Simulations

H. Men* and Z. Fan

BCAST, Brunel University London, Uxbridge, Middlesex, UB8 3PH, UK.

*Corresponding author. E-mail address: hua.men@brunel.ac.uk

ABSTRACT

In this paper, we investigate prenucleation and heterogeneous nucleation in the liquid Pb/solid Al system as an example of systems with large lattice misfit, using molecular dynamics simulation. Solid Pb and Al have a large positive lattice misfit (f) of 18.2% along the densely packed [110] direction. This study reveals that prenucleation occurs at 600 K (an undercooling of 15 K), and a 2-dimensional (2D) ordered structure forms at the interface with a coincidence site lattice (CSL) between the 1st Pb and 1st Al layers. The CSL accommodates the major part of the f , and only a small residual lattice misfit (f_r) of 1.9% remains. The formation of the CSL transforms original substrate into a considerably potent nucleant, where the 1st Pb layer becomes the new surface layer of the substrate. At an undercooling of about 22 K, nucleation proceeds by merging 2D ordered structure through structural templating: the 2nd Pb layer is epitaxial to the CSL Pb layer, the 3rd Pb layer largely accommodates the f_r , and the 4th Pb layer is a nearly perfect crystalline plane. Further analysis indicates that the interface with the CSL has a lower interfacial energy than with a cube-to-cube orientation relationship. For the first time, we established that the CSL was an effective mechanism to accommodate the f for systems with large positive misfit. Heterogeneous nucleation is governed not by a single mechanism (misfit dislocations in Turnbull's model), instead by various mechanisms depending on f . This study sheds new light on the atomistic mechanism of heterogeneous nucleation.

Keywords: *Heterogeneous nucleation; Molecular Dynamics simulation; Lattice misfit; Coincidence site lattice; Interface; Interfacial energy*

I. INTRODUCTION

Nucleation (usually heterogeneous nucleation) plays a vital role in the solidification process,¹ and is relevant to many significant industrial practices (such as: drug production² and castings¹) and natural events (such as ice formation³). The classical nucleation theory (CNT) is widely used to describe the nucleation process, qualitatively in general, i.e. the new phase forms by fluctuations of the configuration, composition, energy and so on in disordered liquid based on statistical mechanics.¹ However, there is a large discrepancy between the predictions of the CNT and experimental results. For instance, the predicted nucleation rate in Hg droplets with the CNT is 5 and 35 orders of magnitude lower for the homogeneous and heterogeneous nucleation, respectively, than

those obtained from experiments.⁴ The large discrepancy between the prediction with CNT, and experimental and simulation results has been argued intensely over past decades.^{3,5} Recently, some findings⁶⁻¹⁶ indicate that pronounced atomic ordering may be induced in the liquid at the liquid/substrate interface by the substrate even above the liquidus (this phenomenon is referred to as prenucleation¹³). Real-time observations with high resolution transmission electron microscopy reveal that liquid Al exhibits layering and in-plane atomic ordering within a few atomic layers at the interface with an α -Al₂O₃ substrate, and the Al atoms in the interfacial layer take the hcp sequence of the substrate, not the fcc sequence as in bulk solid Al.^{10,11} These findings seem to be inconsistent with the assumption for the CNT heterogeneous nucleation that the liquid is disordered at the interface. The pronounced atomic ordering at the interface might also be responsible for the large discrepancy between the predictions of the CNT and experimental results for heterogeneous nucleation. Therefore, it is desirable to investigate the atomic arrangements of the liquid at the interface and its effect on heterogeneous nucleation.

Many efforts have been made to understand the nucleation process, with increasing interests in recent years, and some important progress has been achieved.¹⁷⁻³⁰ A non-classical nucleation theory^{18,20} has been proposed in the research chemistry community that amorphous phase may form initially in the solution or liquid, followed by the formation of nuclei inside the amorphous phase, *i.e.*, so-called 2-step nucleation. The epitaxial nucleation model²² suggests that the new phase forms by continuing the lattice of the substrate during the nucleation, where creation of misfit dislocation at the interface accommodates the lattice misfit, f , and that structural templating might be a practical and general mechanism for heterogeneous nucleation. Atomistic simulations have been proved to be a very powerful tool for studies of nucleation, and can be used to reveal the microscopical details of the nucleation process³ and to obtain the nucleation rate with some reliable approaches, such as forward flux sampling^{31,32}. With the use of classical molecular dynamics (MD) simulation with potentials of the embedded atom method (EAM), it has been reported¹² that 2-3 “prefreezing” layers of crystalline Pb form at the liquid Pb/solid Cu (111) interface at 625 K. Similarly, in a previous study we found that a 2-dimensional (2D) ordered structure forms at the liquid/substrate interface through a structural templating mechanism, which is highly dependent on the f .¹³ Using *ab initio* MD simulations,¹⁹ fcc-like ordering is observed within 3 atomic layers at the liquid Al/TiB₂ interface at a small undercooling of 2 K, and its growth is frustrated by the f between α -Al and TiB₂. On the other hand, it is an extremely challenging task for the in-situ observations of the nucleation process to be made due to its very small length and temporal scales.³ The measured nucleation undercooling, ΔT_n , in Al and Al-Cu liquids using synchrotron shows interesting behaviors:^{25,26} the ΔT_n increases gradually with increasing f initially, rises sharply at around $f = 13\%$, and then starts to decrease when the magnitude of f is larger than 13% (e.g. $\Delta T_n = 39.6$ K for $f = 12.9\%$ and 19 K for $f = 25\%$). This appears to be agreed principally with the conclusion from the phase field crystal

modeling of Tóth et al.,²¹ which suggests the potency of the substrate is not a monotonic function of f . All these studies indicate that pre-nucleation at the liquid/substrate interface may have substantial effects on the process of heterogeneous nucleation.

According to the epitaxial nucleation model,²² the atomistic mechanism of heterogeneous nucleation may vary with f : the structural templating mechanism is achieved through creation of misfit dislocations while the magnitude of f is less than a critical misfit, f_c , (theoretical upper limit, 12.5%), and will change beyond f_c . It predicts that the ΔT_n increases gradually with increasing the $|f|$ for $|f| < f_c$, and becomes very large as f approaches f_c .²² Our MD simulation³³ reveals that the misfit dislocation is an effective mechanism among many (e.g. vacancy³⁴) to accommodate f for systems with a small f of up to 10% ($|f| < 12.5\%$ denoted as small misfit, hereafter). A 3-layer nucleation proceeds for small negative f : a partial edge dislocation network in the 1st layer of the 2D ordered structure largely accommodates the f , and a screw dislocation network in the 2nd layer eliminates the distortion and a nearly perfect crystalline plane in the 3rd layer is then created.³³ As a consequence, the potency of the substrate degrades with increasing f , due to the increase in the density of the misfit dislocations at the interface. Using Monte Carlo (MC) simulations of crystal nucleation on a flat crystalline surface in the Lennard-Jones model, Sear et al.²³ found that the surface lattice strongly influences the nucleation rate, and the nucleation rate generally decreases with increasing f for $|f| < 10\%$ and becomes scattered with further increase in f . They reported that nucleation was epitaxial for small f , and the loss of the epitaxy for large f was responsible for how the nucleation rate varied with f .²³ It appears that the prediction using the epitaxial model²² is in accordance with the results of both Sear's and our simulations, and also consistent with experimental observations^{25,26}. On the other hand, Turnbull's model,³⁵ as a dislocation model for the semi-coherent interface between the nucleus and substrate, suggests that the potency of the substrate is inversely proportional to f . This model seems to be applicable only for systems with small f , but inconsistent with large f . For a system with $|f|$ larger than 12.5% (denoted as large misfit, hereafter), however, it is still not clear how the lattice misfit is accommodated at the interface during nucleation so far.

In this study, we intend to clarify the pre-nucleation and the atomistic mechanism of heterogeneous nucleation for systems with large lattice misfit. Solid Pb and Al have a large positive lattice misfit of 18.2% along the densely packed [110] direction of their fcc structure, and is then taken as an example of a system with large lattice misfit. There exists a repulsive interaction between liquid Pb and Al with a positive heat of mixing of 10 kJ/mol,³⁶ and liquid Pb and solid Al are immiscible. With classical MD simulation, Yang et al.³⁷ reported that there were no pre-freezing layers in liquid Pb at the interface with (111) Al substrate above the melting point of Pb, in contrast to the liquid Pb/(111) Cu interface.¹² In experiments, Moore et al.³⁸ observed Pb droplets embedded in an Al matrix solidified by heterogeneous nucleation at an undercooling of about 22 K. The solidified

Pb particles had $\{111\}$ and $\{100\}$ facets, exhibiting a cube-to-cube orientation relationship (OR) with the Al matrix, and the nucleation occurs on the $\{111\}$ facets of the Al matrix. Therefore, it is interesting to examine whether or not pre-nucleation occurred at the liquid Pb/(111)Al interface and how nucleation proceeds in systems with large f .

The objective of this study is to investigate the pre-nucleation and heterogeneous nucleation in the liquid Pb/solid Al, as an example of general cases with large positive lattice misfit, using classical MD simulations.

II. SIMULATION APPROACH

We use EAM potentials for Al-Pb interatomic interactions in the MD simulations,³⁹ performed by the parallel MD program LAMMPS⁴⁰. The melting temperatures calculated with the potentials are 922 K⁴¹ and 615 K³⁹ for Al and Pb, respectively, compared with their experimental values of 933 K and 600.6 K, respectively. The Al substrate has a $\langle 111 \rangle$ surface orientation, with the z -axis being normal to the $\{111\}$ plane. The dimensions of the Al substrate are $96[11\bar{2}] \times 60[\bar{1}10] \times 18[111]$ atomic planes, and the initial dimensions of the Pb sample are $78[11\bar{2}] \times 49[\bar{1}10] \times 27[111]$ atomic planes, with a total of 34,479 atoms in the simulation system. To minimize artifacts in the simulations, we set up the simulation systems with either partially or fully relaxed Al substrates. For the partially relaxed substrate, the atoms in the innermost layer of the Al slab are held being fixed to avoid Brownian motion, and the others are allowed to move freely. For the fully relaxed substrate, all atoms in the substrate are allowed to move freely while the centre-of-mass of the Al slab is constrained. The periodic boundary conditions are imposed in the x ($[11\bar{2}]$)- and y ($[\bar{1}10]$)-directions of the system. Simulations have been carried out for the systems with either the Nose-Hoover NVT or NPT ensemble. A region of vacuum with an extent of 60 Å is inserted with periodic boundary conditions in the z -direction for the NVT ensemble.

During the simulations, the equations of motion are integrated by the Verlet algorithm with a time step of 0.001 ps. The initial system is heated to a temperature of 700 K with a temperature step of 50 K, each equilibrating for 1 ns. The Pb has been confirmed to be liquid at 700 K. The configuration equilibrated at 700 K is then cooled to the desired temperature with in steps of 5 K, and runs for 1 ns at each temperature step. The total energy and trajectory of the simulation system are monitored until nucleation occurs at a temperature of T , denoted as T_{5K} . The configuration that has been equilibrated at $T_{5K} + 5$ K is then cooled to the desired temperature with in steps of 1 K until the nucleation event is observed at the nucleation temperature, T_n . We find that both the systems with fully or partially relaxed substrates exhibit similar nucleation behaviour, and thereby our results and discussion will focus on the systems with a fully relaxed substrate.

The atomic ordering including layering and in-plane atomic ordering at the interface is characterized by the atomic density profile, $\rho(z)$,⁷ and the z -dependent in-plane order parameter, $S(z)$,⁴² respectively, where z is the distance away from the interface. $\rho(z)$ is expressed as:⁷

$$\rho(z) = \frac{\langle N_z \rangle}{L_x L_y \Delta z}, \quad (1)$$

where N_z is the number of atoms between $z-\Delta z/2$ and $z+\Delta z/2$ at time t , Δz is the width of the bin, which is a 10th of the layer spacing in this study. The angled brackets indicate a time-averaged quantity, and L_x and L_y are the x and y dimensions of the cell. The in-plane order parameter, $S(z)$, is defined as:⁴²

$$S(z) = \frac{\left| \sum_{j \in \Delta z} \exp(i\mathbf{K} \cdot \mathbf{r}_j) \right|^2}{N_z^2}, \quad (2)$$

where the summation is over all atoms labelled j within a given bin of width, Δz , of one layer spacing and \mathbf{K} is a reciprocal lattice vector and \mathbf{r}_j is the position vector of the j^{th} atom in Cartesian space. The details for calculating $\rho(z)$ and $S(z)$ are referred to in Ref. 13.

We employ the time-averaged atomic positions approach and local bond-order analysis to investigate the atomic arrangements in the Pb at the interface. To perform the local bond-order analysis, the local bond-order parameters, $\mathbf{q}_l(i)$, are calculated as:⁴³

$$\mathbf{q}_l(i) = \left(\frac{4\pi}{2l+1} \sum_{m=-l}^l |\mathbf{q}_{lm}(i)|^2 \right)^{\frac{1}{2}}, \quad (3)$$

where the $(2l+1)$ dimensional complex vector $\mathbf{q}_{lm}(i)$ is the sum of spherical harmonics, $Y_{lm}(r_{ij})$, over all the nearest neighbouring atoms of the atom i . The two neighbouring atoms i and j are recognised to be connected if the correlation function, $\mathbf{q}_6(i) \cdot \mathbf{q}_6(j)$, exceeds a threshold of 0.5. A threshold on the number of the connections is set to 6 to distinguish solid atoms from liquid atoms.

The interfacial free energy, γ , of the Pb/Al system can be computed using one of the widely used approaches:⁴⁴⁻⁴⁶

$$\gamma = \{E_{\text{Pb/Al}} - E_{\text{Pb}}^{\text{bulk}} - E_{\text{Al}}^{\text{bulk}}\} / A_{\text{int}} - \sigma_{\text{Pb}} - \sigma_{\text{Al}} \quad (4)$$

where $E_{\text{Pb/Al}}$ is the Helmholtz free energy of the Pb/Al system, and $E_{\text{Pb}}^{\text{bulk}}, E_{\text{Al}}^{\text{bulk}}$ are the free energy of the bulk Pb and Al, respectively, and A_{int} is the area of the interface. $\sigma_{\text{Pb}}, \sigma_{\text{Al}}$ are the surface energy of Pb and Al slabs, respectively:

$$\sigma_m = \{E_m^{\text{vac}} - E_m^{\text{bulk}}\} / 2A_{\text{int}} \quad (5)$$

where E_m^{vac} is the free energy of the slab m with vacuum, and m is Pb or Al. To calculate the E_m^{vac} and E_m^{bulk} , the slabs with vacuum and the bulk Pb and Al are constructed with the same configurations as the Pb/Al system. The simulation systems of Pb and Al are heated from 0.01 K to 900 K with a temperature step of 50 K, equilibrated for 1 ns at each temperature step. We confirmed that the Pb was liquid for either the bulk or the slab with vacuum at 900 K. The liquid Pb is then cooled from 900 K to 600 K with a temperature step of 50 K, equilibrating for 1 ns at each temperature step.

III. RESULTS AND DISCUSSION

A. Atomic ordering at the liquid/substrate interface

Fig. 1a shows the front view of the snapshot of the liquid Pb/solid Al (Pb(l)/Al(s)) system with a fully relaxed substrate (the same configuration is used for discussion hereafter unless we stated otherwise) equilibrated at 625 K using the NVT ensemble. The liquid Pb exhibits a layered structure within a few atomic layers at the interface. The top views of the time-averaged atomic positions of the 1st Al (L1Al) and the 1st Pb (L1Pb) to 3rd Pb (L3Pb) interfacial layers are displayed in Fig. 1b-e. The L1Al has a well-ordered structure, which is identical to the (111) plane of the bulk Al. The atoms in the L1Pb to L3Pb are largely disordered, with only a little ordered structure present in the L1Pb.

Fig. 2a exhibits the density profile, $\rho(z)$, of the system as a function of distance, z , away from the interface. The dashed line represents the interface between the liquid Pb and solid Al. The first 3 atomic layers of the Al at the interface have a slightly low peak density, compared with those of the bulk substrate. The layering of the liquid Pb persists within 6 atomic layers at the interface, with an exponentially decreasing peak density away from the interface. The in-plane order parameter, $S(z)$, of the liquid Pb at the interface as a function of z from the interface is shown in Fig. 2b. The L1Pb to L3Pb have a very low $S(z)$ of about 0.03, just slightly larger than the bulk Pb liquid. This further indicates a largely disordered structure in the liquid Pb at the interface.

We performed a local-bond order analysis to identify the solid and liquid atoms in the simulation system. It is surprising that the L1Pb has a relatively high solid fraction, x_{sol} , of 0.62 at $T = 625$ K, as shown in Fig. 3, although it exhibits a largely disordered structure (Figs. 1c&2b). On the other hand, the x_{sol} of the L2Pb and L3Pb is very low, at 0.1 and 0.01, respectively, suggesting that most of the atoms in the L2Pb and L3Pb are in the liquid state.

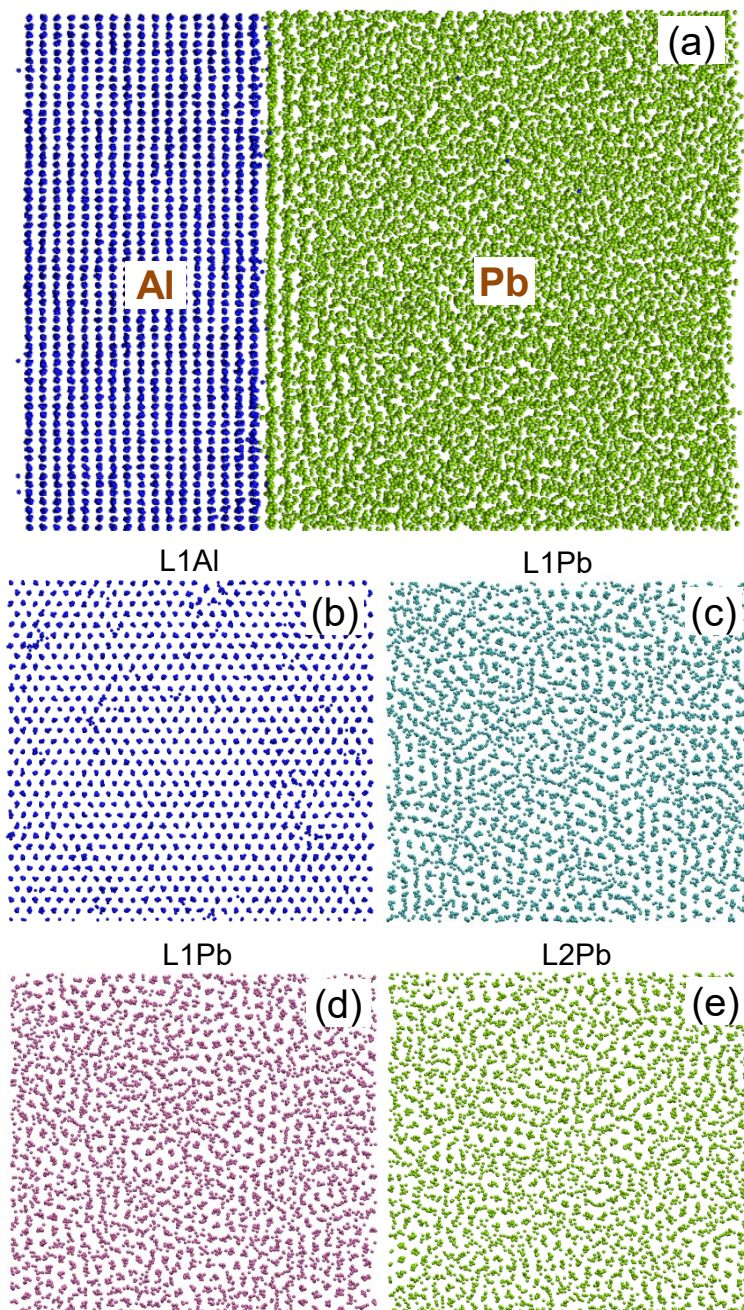


FIG. 1. (a) The front view of the snapshot of the simulation system, and (b-e) top views of the time-averaged atomic positions of the 1st Al layer (L1Al), and 1st (L1Pb), 2nd (L2Pb) and 3rd (L3Pb) Pb layers at the interface in the liquid Pb/solid Al (Pb(l)/Al(s)) system with a fully relaxed substrate equilibrated at 625 K using the NVT ensemble. A layered structure in the liquid Pb at the interface is exhibited, with only a little order present in the L1Pb.

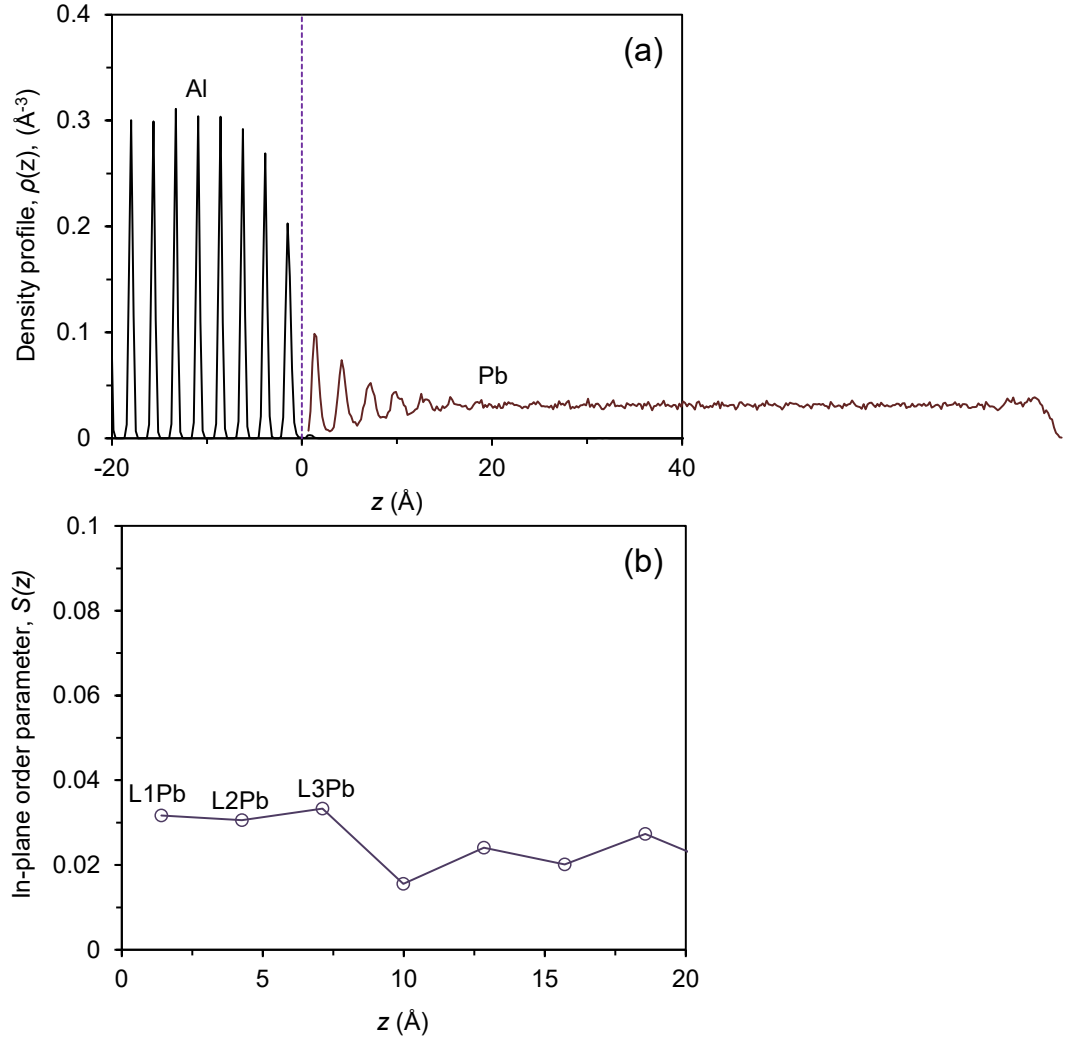


FIG. 2. (a) Density profile, $\rho(z)$, and (b) in-plane order parameter, $S(z)$, as a function of the distance, z , away from the interface for the Pb(*l*)/Al(*s*) system equilibrated at 625 K using the NVT ensemble. The vertical dashed line represents the interface of liquid Pb and solid Al. Layering of the Pb(*l*) persists within 6 atomic layers at the interface, where the liquid Pb has a very weak in-plane atomic ordering.

We conclude that no 2D ordered structure exists in the liquid Pb at the interface at $T = 625$ K. This agrees well with the observation of Yang *et al.*^{37,47} that no prefreezing layers are found in Pb/Al interfaces of any orientation above the liquidus. This might be attributed to the repulsive interaction and large lattice misfit between Pb and Al. However, we found that there was a substantial solid fraction in the L1Pb even above the T_1 of the Pb. It has been reported that liquid Pb atoms can be captured at the interface by the lattice of Si substrate, where these Pb atoms may be stabilized at the equilibrium atomic positions

provided by the lattice of a surface layer of the Si substrate.⁴⁸ Consequently, these atoms lose the characteristics of the liquid atoms (i.e., moving around) and vibrate at the equilibrium atomic positions like solid atoms. This could be the reason that the solid Pb atoms accounts for a high proportion of the L1Pb in the Pb(*l*)/Al(*s*), which can be located at the individual equilibrium atomic positions provided by the L1Al, but have little ordered structure due to its large atomic size.

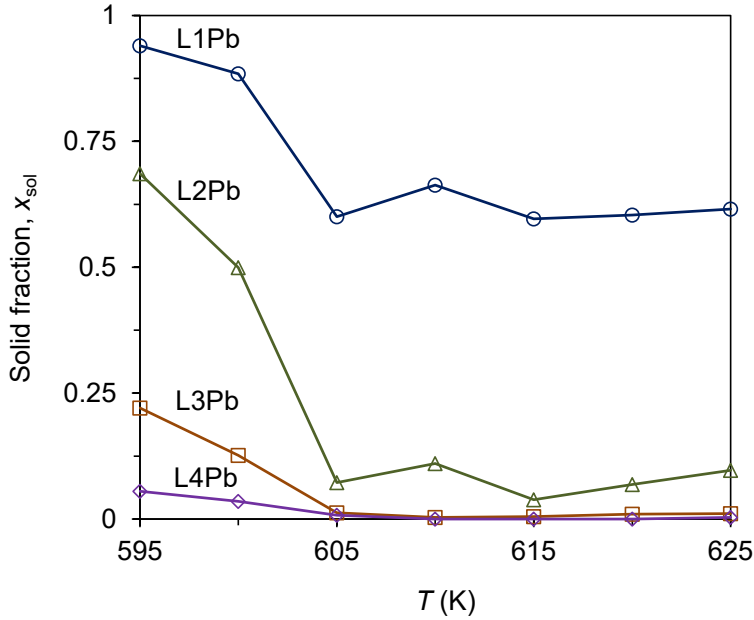


FIG. 3. Variation in the solid fraction, x_{sol} , of the individual layers in the liquid Pb at the interface as a function of T for the Pb(*l*)/Al(*s*) system under annealing using the NVT ensemble. The x_{sol} of the L1Pb to L3Pb remains almost unchanged from $T = 625$ K to 605 K, and increases significantly at 600 K.

B. Prenucleation

On annealing from $T = 625$ K to 605 K with a temperature step of 5 K, the total energy, E_t , of the Pb(*l*)/Al(*s*) system remains constant during the equilibration at each T , and decreases linearly as a function of T . As an example, Fig. 4a shows E_t as a function of time, t , during the equilibration at $T = 605$ K, where the horizontal solid line is used to indicate the variation of the E_t during the simulation. Fig. 5a displays the time-averaged atomic positions of the L1Pb/L1Al, L2Pb and L3Pb at $T = 605$ K. The atomic ordering in the L1Pb at $T = 605$ K enhances marginally, compared to $T = 625$ K (Fig. 1c), and the L2Pb and L3Pb still have a disordered structure. Thus, no 2D ordered structure forms at the interface in the Pb(*l*)/Al(*s*) system until T decreases to 605 K during the cooling.

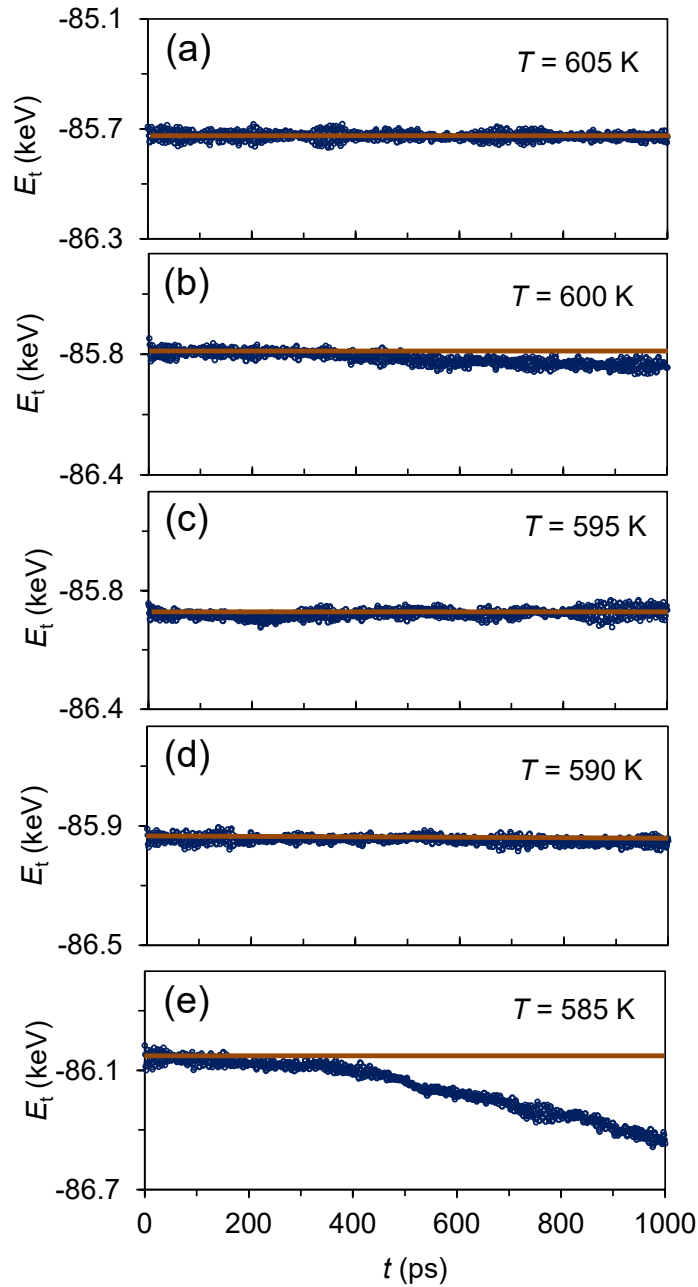


FIG. 4. Total energy, E_t , as a function of time, t , for the Pb(l)/Al(s) system at (a) $T = 605$ K, (b) 600 K, (c) 595 K, (d) 590 K and (e) 585 K during the annealing with a temperature step of 5 K. The horizontal solid lines are used to indicate the variation in the E_t with t . The E_t decreases slightly with t during the simulation for 600 K, and drops markedly by the end of the simulation at $T = 590$ K.

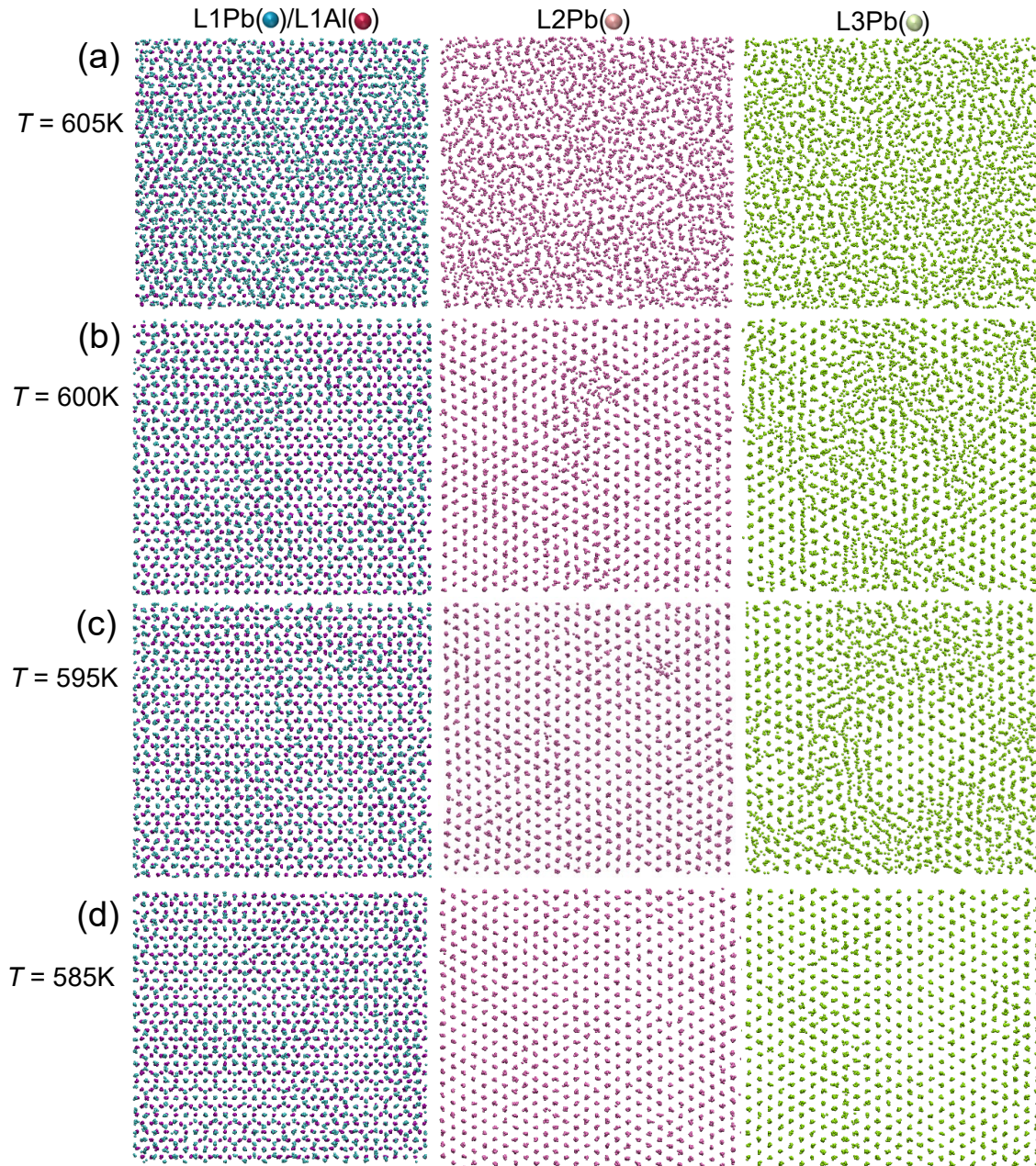


FIG. 5. Time-averaged atomic positions of the L1Pb/L1Al to L3Pb in the Pb(*l*)/Al(*s*) system, using the NVT ensemble at $t = 1000$ ps during the simulations for (a) $T = 605$ K, (b) 600 K, (c) 595 K and (d) 585 K, respectively. At 600 K, hexagonal patterns in the L1Pb/L1Al (the Al and Pb atoms are located on different atomic planes) and a 2-dimensional (2D) ordered structure at the interface form. At 585 K, the L1Pb to L3Pb become completely ordered. The hexagonal patterns in the L1Pb/L1Al mark the formation of the coincidence site lattice (CSL), and the L1Pb is denoted as the CSL-Pb layer hereafter.

A marked change is visible during the simulation at $T = 600$ K. The E_t of the Pb(l)/Al(s) system starts to decrease slightly from $t = 200$ ps, and levels off from 800 ps (Fig. 4b). Fig. 5b exhibits the time-averaged atomic positions of the L1Pb/L1Al, L2Pb and L3Pb at $t = 1000$ ps during the simulation for $T = 600$ K. Compared with those at $T = 605$ K, the atomic ordering of the L1Pb to L3Pb increases substantially at $T = 605$ K. The L1Pb and L2Pb have a largely ordered structure, and the L3Pb is a mixed structure with ordered and disordered regions, indicating that a 2D ordered structure forms at the interface. It is interesting to note that hexagonal patterns appear in the L1Pb/L1Al. In the centre of the hexagonal patterns, one Pb atom in the L1Pb sits on top of an underneath Al atom in the L1Al, surrounded by six Pb atoms in the L1Pb and six Al atoms in the L1Al. The 6 Pb atoms in the L1Pb are located at the equilibrium atomic positions provided by the Al atoms in the L1Al. The hexagonal patterns mark the formation of a coincidence site lattice (CSL) between the L1Al and the L1Pb (L1Pb denoted as CSL-Pb layer hereafter), and we will describe it in more detail later. The E_t remains constant during the simulation for $T = 595$ K (Fig. 4c), where the atomic ordering in the liquid Pb at the interface enhances slightly due to the increase in undercooling of 5 K (Fig. 5c). It suggests that there is no significant change in the 2D ordered structure at the interface at 595 K.

The E_t also remains constant during the simulation for $T = 590$ K (Fig. 4d), but drops dramatically from the beginning of the simulation for $T = 585$ K (Fig. 4e). It implies that heterogeneous nucleation starts at the end of the simulation at 590 K during the annealing with a temperature step of 5 K. At 585 K, the first three atomic Pb layers at the interface have been transformed into a completely ordered structure (Fig. 5d). This suggests the nucleation temperature, T_n , for the Pb(l)/Al(s) system will be between 595 K and 590 K.

The variation in the solid fraction, x_{sol} , of the CSL-Pb(L1Pb) to L4Pb as a function of T for annealing from $T = 625$ K to 595 K was plotted in Fig. 3. The x_{sol} of the individual layers at the interface remains nearly constant from $T = 625$ K to 605 K, at about 0.6, 0.1 and 0.01 for the CSL-Pb, L2Pb and L3Pb, respectively, and increases dramatically to 0.88, 0.5 and 0.13, respectively, at 600 K. The remarkable increase in the x_{sol} at $T = 600$ K corresponds to the formation of the hexagonal patterns in the CSL-Pb and the 2D ordered structure at the interface (Fig. 5b). With further undercooling to 595 K, the x_{sol} of the individual layers at the interface increases slightly, and therefore the 2D ordered structure does not trigger nucleation instantly during the cooling.

To examine the formation of the hexagonal patterns in the CSL-Pb, the time-averaged atomic positions of the CSL-Pb/L1Al during the simulation for 600K are displayed in Fig. 6. At $t = 10$ ps, the CSL-Pb has a roughly disordered structure (Fig. 6a). The hexagonal patterns start to appear at $t = 200$ ps (Fig. 6b), and then spread substantially from 300 ps to 700 ps (Fig. 6c-e), and cover nearly the entire CSL-Pb layer at 900 ps (Fig. 6f).

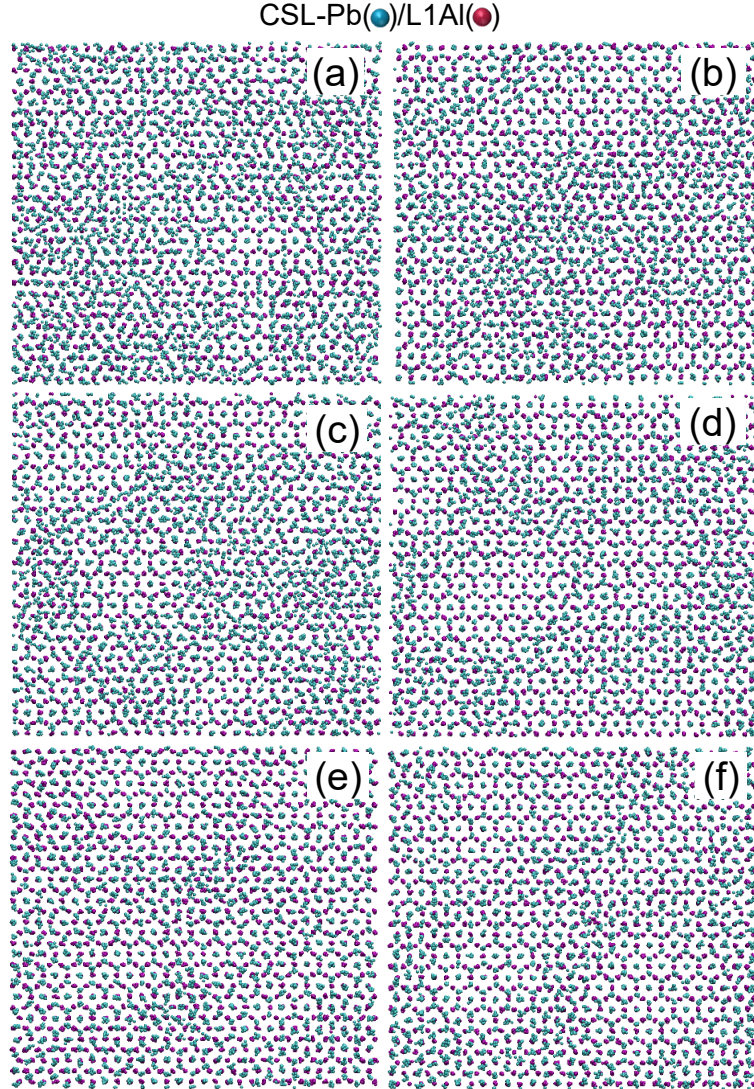


FIG. 6. Time-averaged atomic positions of the CSL-Pb(L1Pb)/L1Al in the Pb(*l*)/Al(*s*) system, using the NVT ensemble at (a) $t = 10$ ps, (b) 200 ps, (c) 300 ps, (d) 400 ps, (e) 700 ps and (f) 900 ps during the simulation for 600 K. The CSL-Pb has a roughly disordered structure at $t = 10$ ps. The hexagonal patterns start to form at 200 ps, and spread significantly from 300 ps to 700 ps and cover nearly the entire CSL-Pb layer at 900 ps.

The hexagonal pattern in the CSL-Pb/L1Al results from the formation of a coincidence

site lattice at the interface. One enlarged region of the snapshot of the CSL-Pb/L1Al at the end of the simulation for $T = 600\text{K}$ is shown in Fig. 7a. There exists a specific OR between the two planes and two independent atomic matching rules (AMRs):

$$\begin{aligned} (111)\langle 110 \rangle_{\text{Pb}} // (111)\langle 211 \rangle_{\text{Al}} & \quad (\text{OR 1}) \\ 3d_{\text{Pb}\langle 110 \rangle} = 2d_{\text{Al}\langle 211 \rangle} & \quad (\text{AMR1}) \\ (111)\langle 211 \rangle_{\text{Pb}} // (111)\langle 110 \rangle_{\text{Al}} & \quad (\text{OR 2}) \\ 1d_{\text{Pb}\langle 211 \rangle} = 2d_{\text{Al}\langle 110 \rangle}, & \quad (\text{AMR2}) \end{aligned}$$

where $d_{m\langle ijk \rangle}$ is the atomic spacing along $\langle ijk \rangle$ direction in the CSL-Pb or L1Al, and m is Pb or Al. According to the symmetry, the specific OR between the CSL-Pb/L1Al can be determined to be a $\Sigma 3$ CSL.^{49,50} A unit cell of the CSL in the CSL-Pb/L1Al (highlighted by the parallelogram in Fig. 7a) is displayed in Fig. 7b. It is worthwhile to note that the densely packed $[\bar{1}10]$ Pb in the CSL-Pb matches with the less densely packed $[\bar{2}11]$ Al in the L1Al with an f of 50%, and the less densely packed $[\bar{2}1\bar{1}]$ Pb in the CSL-Pb matches with the densely packed $[\bar{1}10]$ Al in the L1Al with an f of -50%, as shown schematically in Fig. 7c. The CSL-Pb twists by an angle of 30° relative to the L1Al, suggesting that the $\Sigma 3$ CSL can be obtained simply by rotating the CSL-Pb by 30° around the z -axis relative to the L1Al. In the unit cell, the four Pb atoms in the vertex of the parallelogram sit on top of the underlying Al atoms in the L1Al, which are metastable. The 2 Pb atoms inside the parallelogram are located at the equilibrium positions provided by three underneath Al atoms in the L1Al. Of the total three Pb atoms in the unit cell, two are located at equilibrium atomic positions, and one is at a metastable position. Thus, a considerably good matching between the CSL-Pb and L1Al is achieved by the formation of the CSL.

The atomic spacing, d_a , of the individual layers at the interface is calculated by averaging the distances between all the nearest neighbor atoms in the corresponding layers at the end of the simulation for $T = 600\text{K}$. The L1Al has a d_a of about 2.9 \AA , almost identical to the bulk substrate and the theoretical value (2.89 \AA) of solid Al at $T = 600\text{K}$. On the other hand, the CSL-Pb has a d_a of about 3.47 \AA , slightly smaller than the theoretical value (3.53 \AA) of solid Pb at $T = 600\text{K}$. This suggests that the atoms in the CSL-Pb is under compression, attributed to the compressive stress that the Pb atoms at the interface are subject to due to the large positive lattice misfit between the Pb and substrate.¹²

It is essential for heterogeneous nucleation to accommodate the lattice misfit between the new phase and substrate at the interface. Otherwise, the strain energy in the new phase will accumulate due to the lattice misfit, and make growth of the new phase impossible.²² We obtained the residual lattice misfit, f_r , at the interface after the formation of the CSL by calculating the relative ratio of the average d_a of the CSL-Pb in the CSL and the bulk solid Pb. The detail of the calculation is referred to Refs. 13,22. The calculated f_r is about

1.9%. Compared with $f = 18.2\%$ between the bulk solid Al and Pb along their densely packed $[110]$ direction in the (111) plane, this suggests that the major part of the f of the simulation system has been accommodated by the CSL formed during the prenucleation.

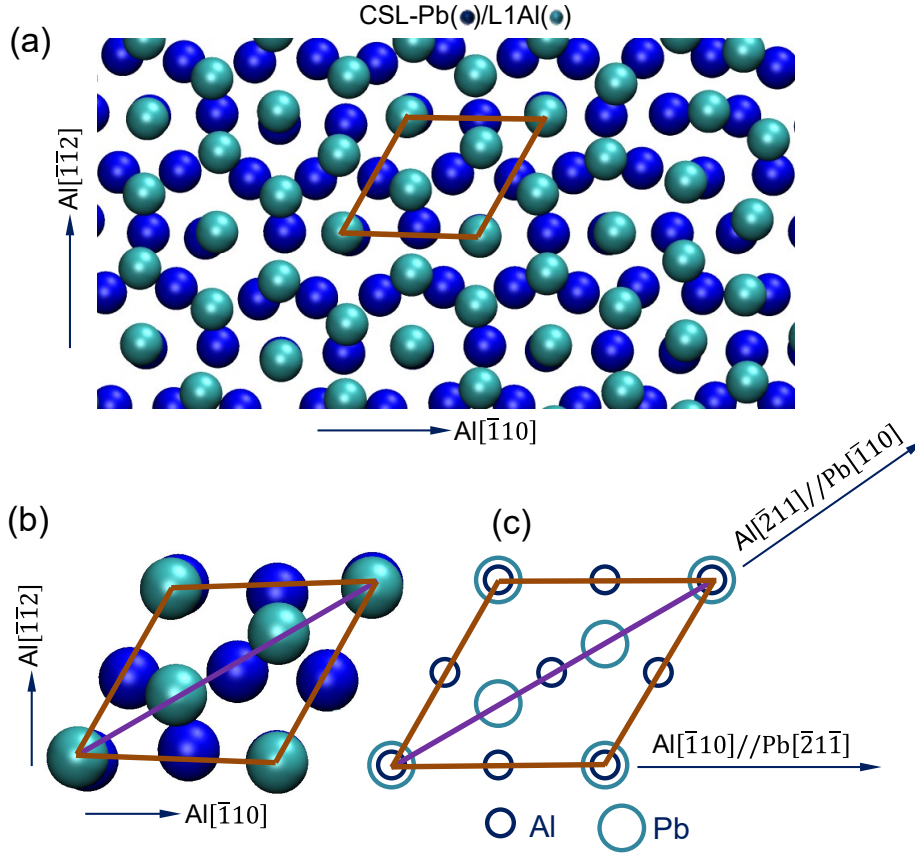


FIG. 7. (a) An enlarged region inside the snapshot of the CSL-Pb/L1Al, and (b) a unit cell of the coincidence site lattice (CSL) and (c) its schematics at $t = 1000$ ps during the simulation for $T = 600$ K for the Pb/Al system using the NVT ensemble. The unit cell of the CSL is highlighted by the parallelogram in (a). In the unit cell, the densely packed $[\bar{1}10]$ Pb in the CSL-Pb matches with the less densely packed $[\bar{2}11]$ Al in the L1Al, and the less densely packed $[\bar{2}1\bar{1}]$ Pb in the CSL-Pb matches with the densely packed $[\bar{1}10]$ Al in the L1Al. A good matching exists between the CSL-Pb and L1Al, indicative of no loss of epitaxy at the interface.

We can conclude that prenucleation occurs in the $\text{Pb}(l)/\text{Al}(s)$ at $T = 600$ K (an undercooling of about 15 K), and a 2D ordered structure forms at the interface. Phenomenologically, prenucleation in this study is analogous to the 1st stage of so-called 2-step nucleation,^{18,20} which suggests that stable prenucleation clusters form in liquids or solutions to serve as the precursor of subsequent nucleation. However, we rather refer to the formation of the 2D ordered structure with the CSL in the $\text{Pb}(l)/\text{Al}(s)$ system as the prenucleation since it cannot trigger the formation of the new phase spontaneously and is thus distinct from the stage of heterogeneous nucleation. Prenucleation is driven by

the reduction of the interfacial energy at the liquid/substrate interface, and thermodynamically in an equilibrium state. This is the reason that the prenucleation can occur even above T_1 .^{13,34,51} Prenucleation appears to be a general phenomenon occurring at liquid/substrate interfaces,^{12,13,33,51} and the atoms in the liquid at the interface may no longer be disordered when heterogeneous nucleation takes place.

This study reveals that the CSL is a very effective mechanism to accommodate f for nucleation systems with large positive lattice misfit, and can dramatically promote the potency of the substrate. In the Pb(*l*)/Al(*s*) system, the major part of f of the system is accommodated by the CSL during prenucleation, and only a small residual lattice misfit of 1.9% is left to be accommodated in the subsequent nucleation. Consequently, the original Al(*s*) is transformed into a new substrate, equivalent to a nucleant having an f of 1.9%, which is considerably potent. The same mechanism has also been found in the Pb(*l*)/Cu(*s*) system,⁵¹ which has a positive f of about 25.3% between bulk solid Pb and Cu along the densely packed [110] direction. The concept of CSL has been widely used to characterize grain boundaries⁴⁹ and the interfacial structure of heterophases in solid precipitation⁵⁰. Our study suggests that the CSL mechanism is also applicable to heterogeneous nucleation at the liquid/substrate interface for the systems with large lattice misfit, where the best matching between the nuclei and the substrate can be achieved by varied Σ numbers of the CSL.

C. Heterogeneous nucleation

During annealing of the Pb(*l*)/Al(*s*) system using the NVT ensemble with a temperature step of 1 K (equivalent to a cooling rate of 10^9 K/s), we further determined that the T_n is 593 K. Fig. 8a exhibits the E_t as a function of the rescaled t during the simulation at $T_n = 593$ K. The E_t remains unchanged before $t = 0$ ps (denoted as t_0), and then decreases continuously. This indicates that nucleation starts at t_0 .

Fig. 8b shows the variation in x_{sol} of the CSL-Pb to L8Pb as a function of the rescaled t during the simulation for $T_n = 593$ K. Before t_0 , the x_{sol} of the individual Pb layers at the interface remains nearly unchanged. This is about 0.95, 0.7, 0.4 and 0.2 for the CSL-Pb to L4Pb, respectively, and close or equal to 0.0 beyond the L4Pb. This suggests that the 2D order structure enhances slightly within four atomic layers at the interface before the occurrence of nucleation with increasing the undercooling as the temperature decrease from $T = 600$ K to 593 K. As soon as nucleation starts at t_0 , the x_{sol} of the individual Pb layers at the interface continues to increase. The x_{sol} of the CSL-Pb increases slightly from 0.95 to 0.98, implying that there is little change in the CSL-Pb during nucleation. It is followed by a dramatic increase in the x_{sol} for further atomic layers, which reaches about 0.9 for the L2Pb to L4Pb within about 0.5 ns after t_0 .

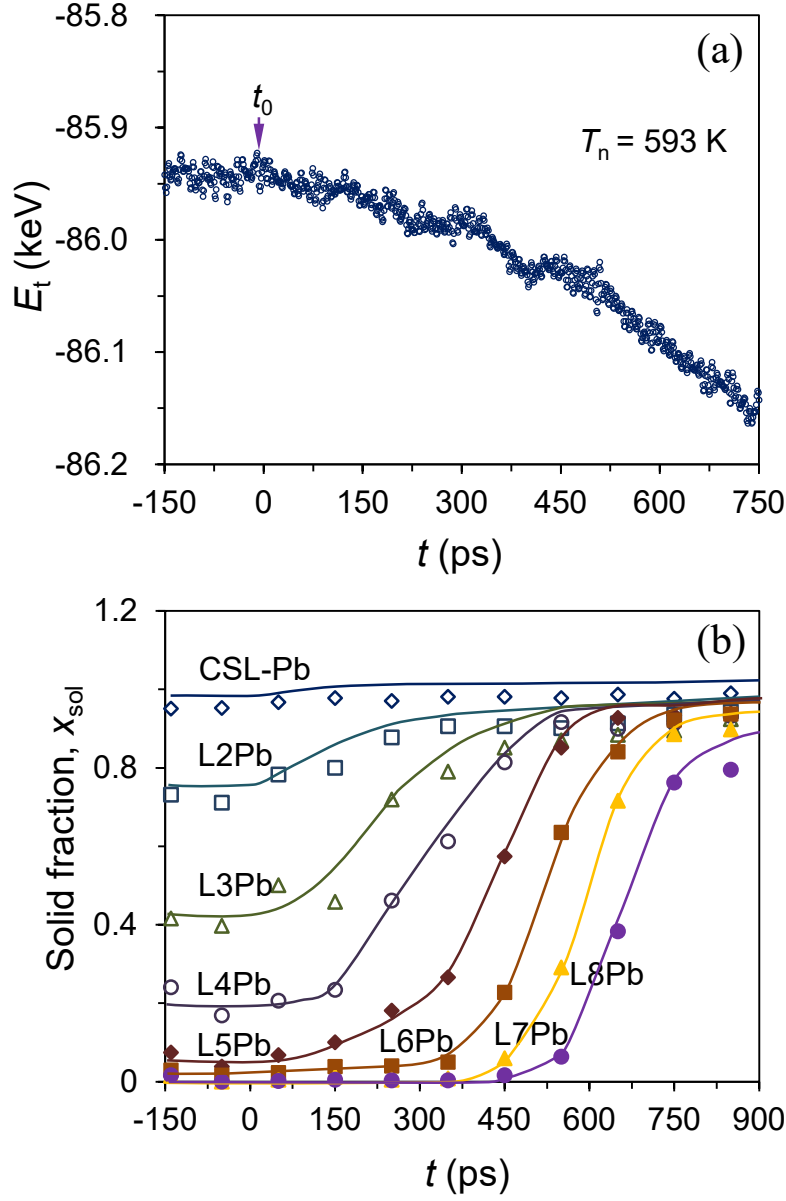


FIG. 8. (a) The E_t of the system and (b) x_{sol} of the individual Pb layers as a function of the rescaled t during the simulation for $T = T_n = 593$ K for the Pb/Al system using the NVT ensemble. Nucleation starts at $t = 0$ ps (denoted as t_0). After t_0 , the x_{sol} of the CSL-Pb increases slightly, and those of further layers at the interface increase dramatically in turn.

To examine the microscopic details of the nucleation, the time-averaged atomic positions of the CSL-Pb/L1Al to L4Pb/L3Pb during the simulation for $T = T_n = 593$ K are displayed in Fig. 9. The hexagonal patterns in the CSL-Pb remain nearly unchanged during the simulation, indicating that the CSL remains intact during nucleation. Before t_0 ($t = 0$ ps), the L2Pb has a largely ordered structure except in some small regions, and the L3Pb and L4Pb have a mixed structure with ordered and disordered regions (Fig. 9a&b). This

suggests that the 2D ordered structure persists in the CSL-Pb to L4Pb until nucleation starts. The ordered structures in the L2Pb to L4Pb begin to merge after t_0 (Fig. 9c). At $t = 450$ ps, the L2Pb to L4Pb have transformed into completely crystalline planes, where the L2Pb and L4Pb are coherent with the CSL-Pb and L3Pb, respectively(Fig. 9d).

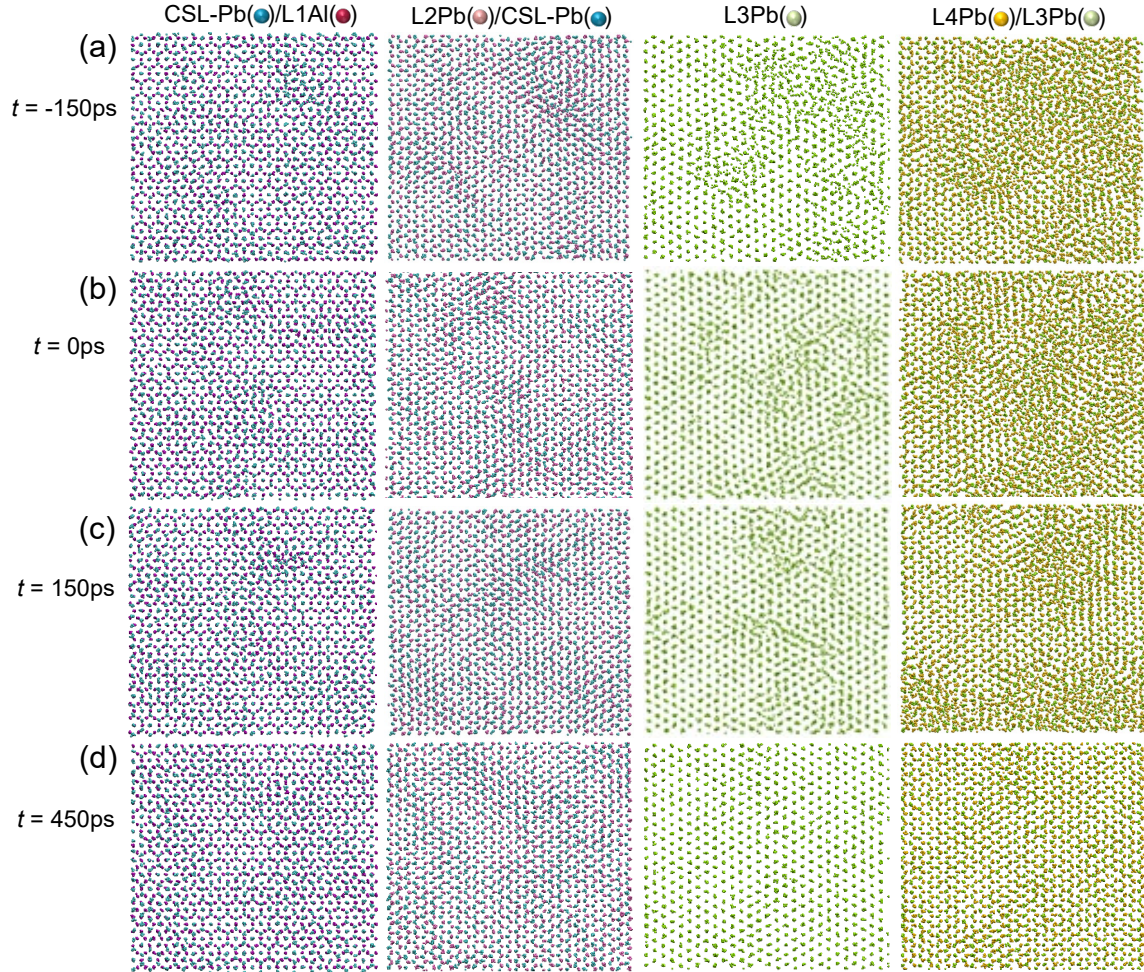


FIG. 9. Time-averaged atomic positions of the L1Al to L4Pb for the Pb/Al system using the NVT ensemble at a rescaled time (a) $t = -150$ ps, (b) 0 ps, (c) 150 ps, (d) 450 ps during the simulation for $T = T_n = 593$ K. The hexagonal patterns in the CSL-Pb/L1Al remains almost unchanged, and the 2D ordered structure at the interface starts to merge after t_0 ($t = 0$ ps).

To investigate how the small residual lattice misfit is accommodated during nucleation, we calculated the accommodated lattice misfit, f_a , of the consecutive Pb layers at the interface at the end of the simulation for $T = T_n = 593$ K. The calculated f_a is about 0.3%, 1.3% and 0% for the L2Pb - L4Pb, respectively. It indicates that the residual lattice misfit is largely accommodated by the L3Pb.⁵¹ The L4Pb is identical to the (111) plane of the solidified bulk Pb, *i.e.*, the L4Pb is an almost perfect crystalline plane.

The nucleation undercooling, ΔT_n , is calculated as $\Delta T_n = T_l - T_n$, where T_l is the melting point (615 K) of Pb based on the potential used in this study.³⁹ The ΔT_n for the Pb(l)/Cu(s) with fully- and partially-relaxed substrates is 22 K and 27 K, respectively, using the NVT ensemble. Fig. 10 displays ΔT_n as a function of the magnitude of f obtained from this and our previous^{33,34,51} studies. ΔT_n increases with increasing f while the magnitude of f is less than 12.5%, but is very low when the magnitude of f is larger than 12.5%. It is interesting to note that the ΔT_n of the Pb(l)/Al(s) system is between those for the systems with $|f| = 1\%$ and 2%. This is in accordance with the small residual lattice misfit of 1.9% in the Pb(l)/Al(s) system after prenucleation, which has to be accommodated in the nucleation. This further indicates that the Al(s) has been transformed into a potent nucleant, with the formation of the CSL at the interface during prenucleation. Therefore, our simulation results are generally consistent with experimental measurements^{25,26}, and agree with the prediction of the epitaxial model²².

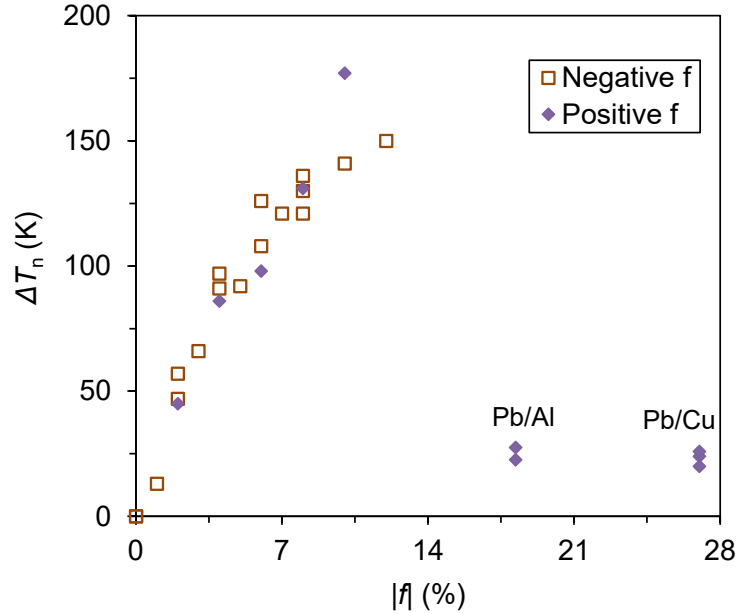


FIG. 10. Nucleation undercooling, ΔT_n , as a function of the magnitude of f obtained from this study and our previous studies^{33,34,51}. The ΔT_n for small lattice misfit is obtained by the simulations on liquid Al/pinned Al substrates, but the lattice parameter of the pinned Al substrate was changed to achieve varied f with either a negative or a positive sign (denoted as Negative f /Positive f , respectively)^{33,34}. ΔT_n initially increases with increasing f for small f and becomes very low for large f , generally consistent with experimental observations^{25,26}.

During solidification, the liquid/solid Pb interface remains rough at an atomic level, as shown in Fig. 11. The solidification of the entire system is not yet completed by the end of the simulation for $T = T_n = 593$ K, where only about nine atomic layers at the interface

have become solid (Fig. 11h). It should be pointed out that the critical size of the nucleus is expected to be very largedue to its small ΔT_n (about 24.1 nm for Pb at an undercooling of 22 K), compared with the size of the cross section (8.6 nm \times 8.0 nm) of the simulation system in this study. Thus, only a fraction of the spherical cap of the nuclei is liable to be observed during solidification, resulting in the finite size effect. The finite size effect is much worse for simulations of systems with very potent substrate since it is highly likely that the critical size of the nucleus is far beyond the size of the simulation system. This is true for most of the MD simulations on heterogeneous nucleation. For instance, Palafox-Hernandez et al.²⁷ reported a layer-by-layer growth without the appearance of a spherical cap during the nucleation of Pb in the Pb(l)/Cu(s) system at an undercooling of 0.5 K. Wang et al.¹⁹ observed one-dimensional growth during nucleation of Al on an Al₃Ti surface with an undercooling of 9 K. Therefore, our interest in this study focuses on the atomistic mechanism of heterogeneous nucleation at the interface, which is fundamentally important to understand the nature of nucleation.

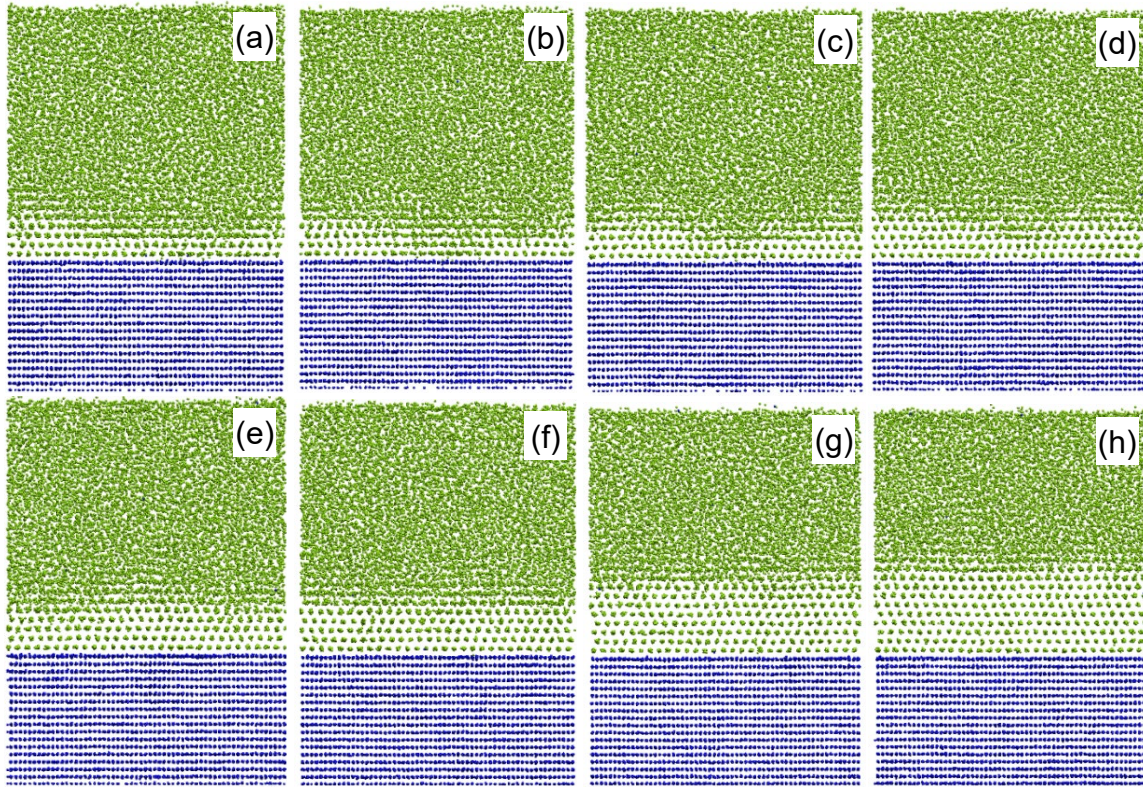


FIG. 11. Front views of snapshots of the Pb/Al system using the NVT ensemble at a rescaled time (a) $t = -150$ ps, (b) -50 ps, (c) 50 ps, (d) 250 ps, (e) 350 ps, (f) 450 ps, (g) 650 ps and (h) 850 ps during the simulation for $T = T_n = 593$ K. The liquid/solid Pb interface remains rough at an atomic level during solidification, and about nine atomic layers become solid by the end of the simulation.

In this study, we have established that structural templating was a general mechanism for

heterogeneous nucleation. Heterogeneous nucleation proceeds by merging 2D ordered structure at the interface, which is formed during prenucleation. It is generally believed that the potency of a substrate degrades with increasing f , as predicted by Turnbull's model³⁵ based on the dislocation mechanism. However, Turnbull's model works only for systems with small f and it does not hold true for large f , according to experimental observations^{25,26,38,52} and simulations^{21,23,27,33,34,51}. Our study suggests that the misfit dislocation is one effective mechanism to accommodate the f during nucleation for systems with small f , for which the potency of the substrate degrades with increasing f .^{33,34} For the systems with large f , the CSL is a very effective mechanism to accommodate the major part of the f during prenucleation, where it provides a good match between the 2D ordered structure and the substrate, and a small residual lattice misfit will be accommodated during nucleation. Therefore, there is no loss of epitaxy during nucleation for large f , in contradiction to Ref. 23. In fact, the abnormality of ΔT_n as a function of f for large f is attributed to the formation of the CSL during prenucleation, instead of loss of the epitaxy at the interface. As a consequence, the substrate can be transformed into a considerably potent nucleant for nucleation, and the structural templating mechanism still works for systems with large f . This is consistent with the prediction of the epitaxial model²², and validated by experimental observations^{25,26,38,52}. Therefore, the heterogeneous nucleation process is governed not by a single mechanism (e.g. Turnbull's model), but by various mechanisms with changing the lattice misfit,^{22,33,51} based on the structural templating. Thereby, it appears that heterogeneous nucleation can be well described by the epitaxial model.²²

D. Interfacial energy

It is interesting to find that a cube-to-cube OR exists at the solid Pb/solid Al interface during heating of the Pb(*s*)/Al(*s*) system, whereas the CSL forms at the liquid Pb/solid Al interface in the prenucleation during cooling the same system. Fig. 12 exhibits the time-averaged atomic positions of the L1Pb(CSL-Pb)/L1Al equilibrated at $T = 300$ K, with NVT ensemble, during heating and cooling. The solid lines in Fig. 12a indicate of a cube-to-cube OR between the bulk solid Pb and Al during heating. The cube-to-cube OR is destroyed when the Pb is completely molten at $T = 650$ K during heating and the system then is fully equilibrated at 700 K. There is little in-plane atomic ordering even in the L1Pb at $T = 625$ K during cooling from $T = 700$ K (Fig. 1c&2b). The CSL forms in the L1Pb/L1Al at $T = 600$ K during annealing (Figs. 4, 5, 6&7), and remains almost unchanged during subsequent nucleation (Fig. 12b). The same phenomenon of the transition from the cube-to-cube OR to the CSL has also been observed during heating and cooling of the system using the NPT ensemble in this study. This suggests that the CSL interface is favoured at the interface during the nucleation process since the cube-to-cube OR during heating is replaced by the CSL OR during cooling.

We calculated the free energy of the solid Pb/solid Al interface with both the

cube-to-cube OR and the CSL as a function of T using Eq. 4, and plotted in Fig. 13. The total interfacial energy, γ , of the solid Pb/solid Al interface with CSL includes the contributions from the CSL and the residual misfit ($f_r = 1.9\%$) in the solid Pb at the interface, denoted as $\gamma_{\text{CSL}+f_r(1.9\%)}$. γ increases with increasing T for both the ORs, and the γ for the cube-to-cube OR ($\gamma_{\text{cube-to-cube}}$) is larger than $\gamma_{\text{CSL}+f_r(1.9\%)}$. For example, $\gamma_{\text{cube-to-cube}}$ is 0.246 J/m^2 at $T = 300 \text{ K}$, compared with 0.183 J/m^2 for $\gamma_{\text{CSL}+f_r(1.9\%)}$. We further calculated the contribution, $\gamma_{f_r(1.9\%)}$, from the strain energy of the residual lattice misfit with $f_r = 1.9\%$ in the solid Pb using the approach of Ref. 22. γ for the interface with the CSL only, γ_{CSL} , is 0.153 J/m^2 at $T = 300 \text{ K}$ after $\gamma_{f_r(1.9\%)}$ is deducted. Thus, γ_{CSL} is less than the $\gamma_{\text{cube-to-cube}}$ at room temperature.

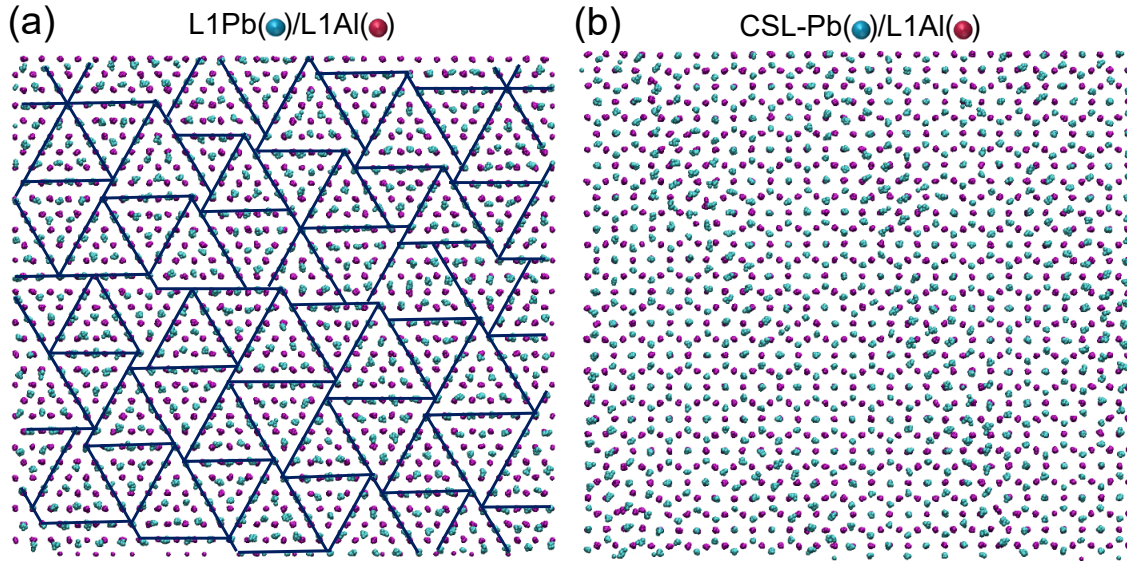


FIG. 12. Time-averaged atomic positions of the L1Pb/L1Al for the Pb/Al system using the NVT ensemble equilibrated at $T = 300 \text{ K}$ during (a) heating and (b) cooling. The solid lines in (a) indicate a cube-to-cube OR between the bulk Pb and Al during heating. During cooling, the CSL forms at the interface (represented by the hexagonal patterns in (b)) in the prenucleation and remains unchanged after nucleation.

γ_{CSL} can also be calculated for the liquid Pb/solid Al interface equilibrated at $T = 600 \text{ K}$ during the cooling, where the CSL forms in the prenucleation. γ for the CSL at $T = 600 \text{ K}$ includes the contributions from the CSL (γ_{CSL}) and the liquid/solid Pb interface ($\gamma_{\text{Pb}}^{\text{LS}}$).

The γ_{CSL} can be obtained from the following equation:

$$\gamma_{\text{CSL}} = \Delta E_t^{21} + \gamma_{\text{AlPb}}^{\text{L}} - \gamma_{\text{Pb}}^{\text{LS}} + \Delta E_{\text{Pb}}^{\text{L} \rightarrow \text{S}} \quad (6)$$

where $\Delta E_t^{21} = E_t^2 - E_t^1$, E_t^1 and E_t^2 are the total energy of the Pb(l)/Al(s) system before and after the formation of the CSL, respectively, during the simulation for $T = 600 \text{ K}$.

$\gamma_{\text{AlPb}}^{\text{L}}$ is the liquid Pb / Al interfacial energy Al before the formation of the CSL. $\Delta E_{\text{Pb}}^{\text{L} \rightarrow \text{S}}$ is the free energy change due to transformation of some liquid atoms to solid atoms at the interface during the formation of the CSL. The calculated γ_{CSL} is 0.31 J/m^2 at $T = 600 \text{ K}$,

which is less than 0.423 J/m^2 for $\gamma_{\text{cube-to-cube}}$, suggesting that γ_{CSL} is smaller than $\gamma_{\text{cube-to-cube}}$ at temperatures close to T_n . Therefore, the CSL is energetically favoured for the solid Pb/(111)Al interface in the nucleation process, compared with the cube-to-cube OR. Furthermore, it is noted that the CSL initially forms at the liquid Pb/solid Al interface in the prenucleation during annealing, and a small residual lattice misfit ($f_r = 1.9\%$) is accommodated during subsequent heterogeneous nucleation. As a consequence, the large positive lattice misfit between solid Pb and solid Al is accommodated by a two-step mechanism: CSL in the prenucleation and a small residual lattice misfit in the nucleation, and might occur more easily than the cube-to-cube OR with a single interface.

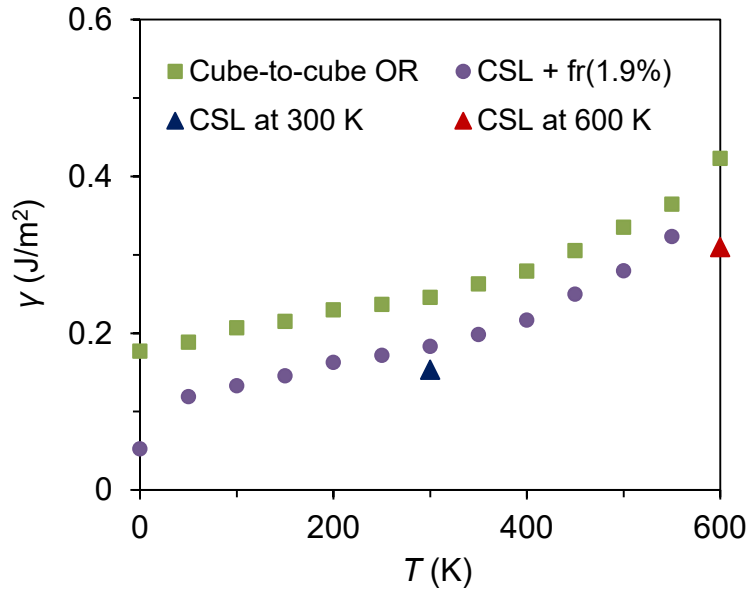


FIG. 13. Calculated interfacial energy, γ , of the (111)Pb/(111)Al interface with a cube-to-cube OR or the CSL + $f_r(1.9\%)$ as a function of T for the Pb/Al system using the NVT ensemble. The $f_r(1.9\%)$ represents the contribution from the strain energy of the residual lattice misfit of $f_r = 1.9\%$ in the solid Pb to the total γ of the interface with the CSL. The γ for the interfaces with CSL-only at $T = 300 \text{ K}$ and 600 K has also been included. The interface with CSL-only has a lower γ than with a cube-to-cube OR.

It has been reported that a cube-to-cube OR exists at the interface for confined Pb particles embedded in an Al matrix, based on transmission electron microscopy (TEM) observation and electron probe microanalysis.³⁸ The confined Pb particles usually exhibited the morphologies with $\{111\}$ and $\{100\}$ facets or curved surfaces,^{38,53-60} with the OR at the interface: $(111)\langle 110 \rangle \text{Pb} // (111)\langle 110 \rangle \text{Al}$.³⁸ The misfit between the Pb and Al is accommodated by a $60^\circ a_0/2 \langle 110 \rangle$ misfit dislocation at about every fifth Al plane,^{61,62} where a_0 is the lattice parameter of the solid Pb. Based on the analysis of nucleation kinetics, Moore et al.³⁸ obtained a contact angle of about 21° , and from it a simple calculation gave $\gamma_{\text{cube-to-cube}} = 0.368 \text{ J/m}^2$ at $T = 578 \text{ K}$, which agrees well with our

simulation result. The MC simulation has also revealed that a cube-to-cube OR exists at the (111) Pb/Al interface, with $\gamma = 0.62 \text{ J/m}^2$ at $T = 300 \text{ K}$,⁶³ which is about twice as large as those determined by us and Moore et al. It is noticed that the cube-to-cube OR observed in the MC simulations is consistent with our result during heating. In both the cases, however, the interfaces with the cube-to-cube OR is not necessarily in the thermodynamically stable state, due to the lack of complete relaxation in either of the simulation systems. In another word, the interface with the cube-to-cube OR may be only in a local minimum of the free energy surface for both the simulation systems, but not a global minimum.

On the other hand, Rösner *et al.* observed an OR of $[110]\text{Pb}/[2\bar{1}1]\text{Al}$ at the (110)Pb/(111)Al interface in the very thin edge of nanometre-sized Pb inclusions and Al matrix after resolidification of the Pb, using in-situ HRTEM.⁶⁴ The misfit is accommodated by $a a_0/2 \langle 110 \rangle$ misfit dislocation at about every fourth Al plane. The authors argued that the $[110]\text{Pb}/[2\bar{1}1]\text{Al}$ OR at the (110)Pb/(111)Al interface was non-equilibrium since it is energetically unfavoured, compared with the ‘classical’ cube-to-cube OR.⁶⁴ It may be attributed to the geometric confinement that the Pb inclusion is subject to at the very thin edge of the sample, where it could be restricted only in 2-dimension by the Al matrix. It is noted that the $[110]\text{Pb}/[2\bar{1}1]\text{Al}$ matching direction at the (110)Pb/(111)Al interface is the same as at the (111)Pb/(111)Al interface in our study, which is better described as the $\Sigma 3$ CSL. To our best knowledge, the CSL interface has the lowest interfacial energy among all the known ORs of the solid Pb/(111)Al interface.

Our MD simulations reveal that a CSL exists at both the top and the bottom interfaces of the completely solidified Pb/Al system during annealing using the NPT ensemble, as shown in Fig. 14. The bulk Pb twists at an angle of 30° relative to the top and bottom bulk Al (Fig. 14b&c). However, such a cryptographic arrangement is forbidden for confined Pb particles embedded in an Al matrix, due to the existence of the (100) facets, although the interface with the CSL is energetically favoured at the (111) facets. Therefore, the existence of a cube-to-cube OR at the interface of the confined Pb/Al matrix does not result from the thermodynamics equilibrium, but instead from the restriction of the geometric confinement. How the confined Pb droplets solidified through heterogeneous nucleation with a cube-to-cube OR on the $\{111\}$ facets of the Al matrix on undercooling remains an open question.

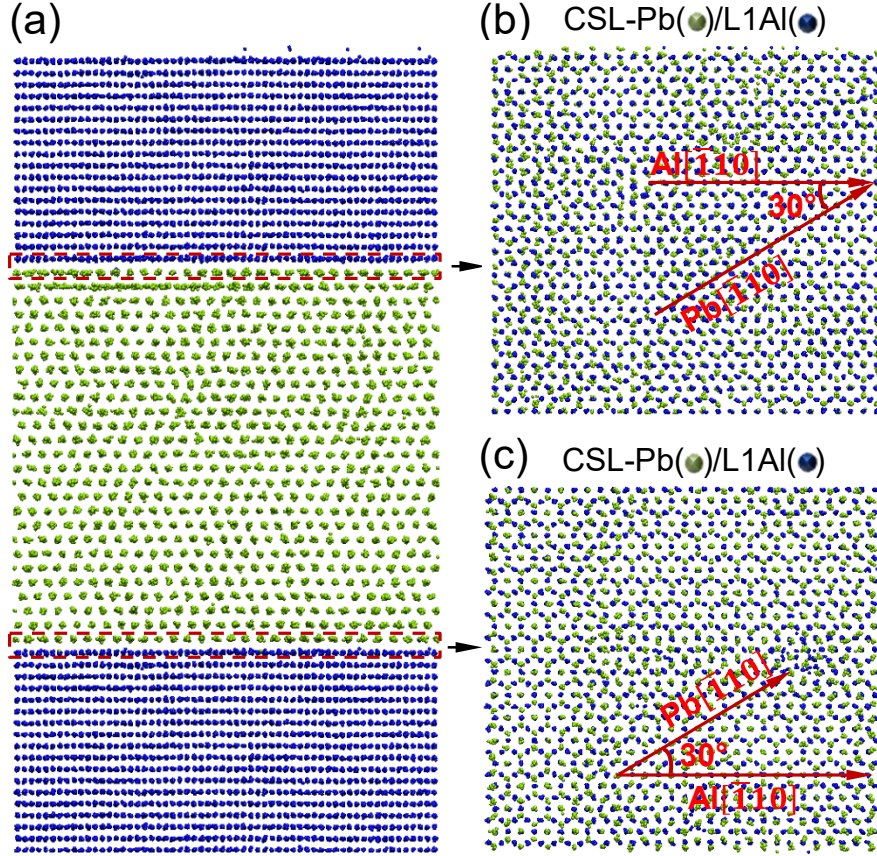


FIG.14.(a) Side view of the snapshot, and top views of the time-averaged atomic positions of (b) top and (c) bottom interfaces for the fully solidified Pb/Al system equilibrated at $T = 550$ K using the NPT ensemble during annealing. The solid arrows in (b) and (c) represent the $[\bar{1}10]$ direction of both Pb and Al. The bulk Pb twists an angle of 30° relative to the top and bottom bulk Al, as indicated by the angle between the two solid arrows. A CSL exists at the CSL-Pb/L1Al of the top and bottom interfaces.

IV. SUMMARY

In this study we investigated prenucleation and heterogeneous nucleation in liquid Pb on a solid Al substrate as an example of systems with large positive lattice misfit, using MD simulations. This study reveals a layered structure exists within six atomic layers in the liquid Pb at the interface, with little in-plane atomic ordering, above its melting point of 615 K. At 600 K, a 2D ordered structure forms at the interface, with a coincidence site lattice (CSL) between the 1st Pb and 1st Al interfacial layers. The CSL accommodates the major part of the lattice misfit of the simulation system, and only a small residual lattice misfit of 1.9% remains in the Pb layer of the CSL. The original Al substrate is transformed into a considerably potent nucleant, with the Pb layer of the CSL becoming the new surface layer of the substrate. Nucleation takes place through merging 2D ordered structure at a relatively small undercooling of about 22 K. It proceeds by a

three-layer nucleation: the 2nd Pb layer is epitaxial to the new surface layer of the substrate; the small residual lattice misfit is largely accommodated by the 3rd Pb layer; and the 4th Pb layer is a nearly perfect crystalline plane. By analyzing the interfacial energy of the Pb/Al interface, it was demonstrated that the interface with the CSL has the lowest interfacial energy among those with (111)Al, and the cube-to-cube OR at confined Pb/Al matrix interface is attributed to the restriction of the geometric confinement. For the first time, we establish that the CSL is a very effective mechanism to accommodate the lattice misfit during heterogeneous nucleation for systems with large positive lattice misfit. Heterogeneous nucleation is governed not by a single mechanism (e.g. misfit dislocations in Turnbull's model), but by various mechanisms with changing lattice misfit.

ACKNOWLEDGMENTS

The author H.M. likes to give thanks to Dr. Ian Stone for reading the manuscript and constructive suggestions on English writing. The EPSRC is gratefully acknowledged for providing financial support under Grant EP/N007638/1. We are grateful to the UK Materials and Molecular Modelling Hub for computational resources, which is partially funded by EPSRC (EP/P020194/1 and EP/T022213/1), and maintained with support from Brunel University London.

AUTHOR'S CONTRIBUTIONS

All authors contributed equally to this work.

DATA AVAILABILITY

The data that supports the findings of this study are available within the article.

NO CONFLICTS OF INTEREST

The authors have no conflicts to disclose.

REFERENCES

- ¹K.F. Kelton, and A.L. Greer, *Nucleation in condensed matter: Applications in materials and biology*, Pergamon, Oxford, 2010.
- ²D. Erdemir, A.Y. Lee, and A.S. Myerson, *Curr. Opin. Drug. Discov. Devel.* 10, 746 (2007).
- ³G.C. Sosso, J. Chen, S.J. Cox, M. Fitzner, P. Pedevilla, A. Zen, and A. Michaelides, *Chem. Rev.* 116, 7078 (2016).
- ⁴D. Turnbull, *J. Chem. Phys.* 20, 411 (1952).

-
- ⁵S. Auer, and D. Frenke, *Nature* 409, 1020 (2001).
- ⁶P. Geysersmans, D. Gorse, and V. Pontikis, *J. Chem. Phys.* 113, 6382(2000).
- ⁷A. Hashibon, J. Adler, M.W. Finnis, and W.D. Kaplan, *Interface Sci.* 9, 175 (2001).
- ⁸A. Hashibon, J. Adler, M.W. Finnis, and W.D. Kaplan, *Comput. Mater. Sci.* 24, 443(2002).
- ⁹W.D. Kaplan, and Y. Kauffmann, *Annu. Rev. Mater. Res.* 36, 1 (2006).
- ¹⁰S.H. Oh, C. Scheu, and M. Rühle, *Korean J. Electron Microscopy Special Issue* 1, 19 (2006).
- ¹¹Y. Kauffmann, S.H. Oh, C.T. Koch, A. Hashibon, C. Scheu, M. Rühle, and W.D. Kaplan, *Acta Mater.* 59, 4378 (2011).
- ¹²J.P. Palafox-Hernandez, B.B. Laird, and M. Asta, *Acta Mater.* 59, 3137 (2011).
- ¹³H. Men, and Z. Fan, *Metall. Mater. Trans. A* 49, 2766 (2018).
- ¹⁴B. Jiang, H. Men, and Z. Fan, *Comput. Mater. Sci.* 153, 73(2018).
- ¹⁵C.M. Fang, H. Men, and Z. Fan, *Metall. Mater. Trans. A* 49, 6231(2018).
- ¹⁶A.L. Greer, *Nature Mater.* 5, 13(2006).
- ¹⁷L. Gránásy, T. Pusztai, D. Saylor, and J.A. Warren, *Phys. Rev. Lett.* 98, 035703 (2007).
- ¹⁸D. Gebauer, A. Völkel, and H. Cölfen, *Science* 322, 1819 (2008).
- ¹⁹J.S. Wang, A. Horsfield, U. Schwingenschlögl, and P.D. Lee, *Phys. Rev. B* 82, 184203 (2010).
- ²⁰P.G. Vekilov, *Nanoscale* 2, 2346 (2010).

-
- ²¹G.I. Tóth, G. Tegze, T. Pusztai, and L. Gránásy, *Phys. Rev. Lett.* 108, 025502(2012).
- ²²Z.Fan, *Metall. Mater. Trans. A44*, 1409 (2013).
- ²³J.P. Mithen, and R.P. Sear, *J. Chem. Phys.* 140, 084504(2014).
- ²⁴R. Cabriolu, and T.S. Li, *Phys. Rev. E* 91, 052402(2015).
- ²⁵L. Wang, L. Yang, D. Zhang, M. Xia, Y. Wang, and J.G.Li, *Metall. Mater. Trans. A47*, 5012 (2016).
- ²⁶L. Wang, W.Q. Lu, Q.D. Hu, M.X. Xia, Y. Wang, and J.G.Li, *Acta Mater.* 139, 75 (2017).
- ²⁷J.P. Palafox-Hernandez, and B.B. Laird, *J. Chem. Phys.* 145, 211914(2016).
- ²⁸G.C.Sosso, T.Li, D.Donadio, G.A.Tribello, and A.Michaelides, *J. Phys. Chem. Lett.* 7, 2350 (2016).
- ²⁹H.H. Lin, T. Li, and H. Li, *Phys. Chem. Chem. Phys.* 20, 29856(2018).
- ³⁰T. Fujinaga, and Y. Shibuta, *Comput. Mater. Sci.*164, 74(2019).
- ³¹R.J. Allen, P.B. Warren, and P.R. ten Wolde, *Phys. Rev. Lett.* 94, 018104 (2005).
- ³²S. Hussain, A. Haji-Akbari, *J. Chem. Phys.* 152, 060901 (2020).
- ³³Z. Fan, H. Men, Y. Wang, and Z.P. Que, *metals* 11, 478(2021).
- ³⁴Z. Fan, and H. Men, *Mater. Res. Express* 7, 126501 (2020).
- ³⁵D. Turnbull, and B.Vonnegut, *Ind. Eng. Chem.* 44, 1292 (1952).
- ³⁶A. Takeuchi, and A. Inoue, *Mater. Trans.* 46, 2817 (2005).
- ³⁷Y.Yang, D.L. Olmsted, M.Asta, and B.B.Laird, *Acta Mater.* 60, 4960 (2012).
- ³⁸K.I. Moore, D.L. Zhang, and B. Cantor, *Acta Metall. Mater.* 38, 1327 (1990).

-
- ³⁹A.Landa, P.Wynblatt, D.J. Siegel, J.B. Adams, O.N.Mryasov, and X.-Y. Liu, *Acta Mater.* 48, 1753 (2000).
- ⁴⁰S. Plimpton, *J. Comput. Phys.* 117, 1 (1995).
- ⁴¹J.R. Morris, C.Z. Wang, K.M. Ho, and C.T.Chan, *Phys. Rev. B* 49, 3109 (1994).
- ⁴²J.R. Hook, H.E. Hall, *Solid State Physics*, second ed., Wiley, Chichester, 1991.
- ⁴³P.J. Steinhardt, D.R. Nelson, and M.Ronchetti, *Phys. Rev. B* 28, 784 (1983).
- ⁴⁴Y. Ortega, D.F. Hevia, J. Oviedo, and M.A. San-Miguel, *Appl. Surf. Sci.* 294, 42-48 (2014).
- ⁴⁵K. Parlinski, *Phys. Rev. B* 74, 184309 (2006).
- ⁴⁶D. Matsunaka, and Y. Shibutani, *Phys. Rev. B* 77, 165435 (2008).
- ⁴⁷Y. Yang, and B.B.Laird, *J. Phys. Chem. B* 118, 8373 (2014).
- ⁴⁸K.A. Jackson, *Interface Sci.* 10, 159 (2002).
- ⁴⁹S. Ranganathan, *Acta Cryst.* 21, 197 (1966).
- ⁵⁰W.-Z. Zhang, and G.C. Weatherly, *Progress in Materials Science* 50, 181 (2005).
- ⁵¹H. Men, and Z. Fan, *metals* 12, 1583 (2022).
- ⁵²W.T. Kim, and B. Cantor, *Acta Metall. Mater.* 40, 3339 (1992).
- ⁵³P.A. Thackery, and R.S. Nelson, *Phil. Mag.* 19, 169 (1969).
- ⁵⁴K.I. Moore, K. Chattopadhyay, and B. Cantor, *Proc. R Soc. A* 414 499 (1987).
- ⁵⁵D.L. Zhang, and B. Cantor, *Acta Metall. Mater.* 39, 1595 (1991).
- ⁵⁶H.W. Sheng, G. Ren, L.M. Peng, Z.Q. Hu, and K. Lu, *Phil. Mag. Lett.* 73, 179 (1996).

-
- ⁵⁷U. Dahmen, S.Q. Xiao, S. Paciornik, E. Johnson, and A. Johansen, *Phys. Rev. Lett.* 78, 471 (1997).
- ⁵⁸E. Johnson, A. Johansen, U. Dahmen, S. Chen, and T. Fujii, *Mater. Sci. Eng. A* 304-306, 187 (2001).
- ⁵⁹H. Gabrisch, L. Kjeldgaard, E. Johnson, and U. Dahmen, *Acta Mater.* 49 4259 (2001).
- ⁶⁰H. Rösner, P. Scheer, J. Weissmüller, and G. Wilde, *Phil. Mag. Lett.* 83, 511-523 (2003).
- ⁶¹H. Rösner, J. Weissmüller, and G. Wilde, *Phil. Mag. Lett.* 84, 673 (2004).
- ⁶²H. Rösner, J. Weissmüller, and G. Wilde, *Phil. Mag. Lett.* 86, 623 (2006).
- ⁶³A. Landa, P. Wynblatt, E. Johnson, and U. Dahmen, *Acta mater.* 48, 2557-2563 (2000).
- ⁶⁴H. Rösner, B. Freitag, and G. Wilde, *Phil. Mag. Lett.* 87, 341 (2007).